

Article

Rotational Maneuvers of Copepod Nauplii at Low Reynolds Number

Kacie T. M. Niimoto ^{1,2}, Kyleigh J. Kuball ¹, Lauren N. Block ¹, Petra H. Lenz ¹ and Daisuke Takagi ^{1,2,3,*} 

¹ Bekey Laboratory of Neurobiology, Pacific Biosciences Research Center, University of Hawaii at Manoa, Honolulu, HI 96822, USA; ktmn@hawaii.edu (K.T.M.N.); kyleighk@hawaii.edu (K.J.K.); blockln7@hawaii.edu (L.N.B.); petra@hawaii.edu (P.H.L.)

² Department of Mechanical Engineering, University of Hawaii at Manoa, Honolulu, HI 96822, USA

³ Department of Mathematics, University of Hawaii at Manoa, Honolulu, HI 96822, USA

* Correspondence: dtakagi@hawaii.edu

Received: 1 April 2020; Accepted: 18 May 2020; Published: 21 May 2020



Abstract: Copepods are agile microcrustaceans that are capable of maneuvering freely in water. However, the physical mechanisms driving their rotational motion are not entirely clear in small larvae (nauplii). Here we report high-speed video observations of copepod nauplii performing acrobatic feats with three pairs of appendages. Our results show rotations about three principal axes of the body: yaw, roll, and pitch. The yaw rotation turns the body to one side and results in a circular swimming path. The roll rotation consists of the body spiraling around a nearly linear path, similar to an aileron roll of an airplane. We interpret the yaw and roll rotations to be facilitated by appendage pronation or supination. The pitch rotation consists of flipping on the spot in a maneuver that resembles a backflip somersault. The pitch rotation involved tail bending and was not observed in the earliest stages of nauplii. The maneuvering strategies adopted by plankton may inspire the design of microscopic robots, equipped with suitable controls for reorienting autonomously in three dimensions.

Keywords: locomotion; reorientation; swimming microorganism

1. Introduction

Animals change the orientation of their body by coordinating the movements of various body parts. For animals capable of moving quickly with considerable inertia through air or water, they may rotate easily with minor body adjustments, as demonstrated by fruit flies [1] and spinner dolphins [2]. For microscopic organisms with small inertia, however, they must actively and repeatedly move their body parts in order to rotate adequately in fluids dominated by viscosity. In this physical regime of low Reynolds number (Re), it is well known that bacteria can tumble [3], and phototactic algae can reorient [4], using flexible flagella. However, microcrustaceans such as larval copepods have relatively stiff bodies and appendages. They have been observed to turn sharply, but their rotational motion is not as well understood as their translational motion [5,6]. Thus, further research is needed to unravel the physical mechanisms underlying the rotational motion of larval copepods.

Numerous theoretical and physical models have considered the problem of reorientation with rigid body parts at low Reynolds number. A key constraint on bodies with minimal inertia is that they cannot translate or rotate by themselves through movements that are reversible in time [7]. Cycles of irreversible kinematic changes are needed to reorient, and this requires at least two degrees of freedom. One of the simplest models of a reorienting body consists of three spheres, each connected to a rigid rod of equal length, with the rods meeting at a common point [8]. The whole system can rotate through an

irreversible sequence of cyclical changes in the angles between the rods. Other examples of reorienting bodies include three rigid spheres that are arranged in a triangle and connected by springs, which are stretched and compressed in sequential order [9], and a pair of paddles, fitted with disks at each end, driven to rotate, with adjustable spacing between the paddles [10]. These simple swimmers have elucidated the minimal components needed for reorienting. Still, their maneuverability is limited and inefficient because many cycles of body movements are typically needed, e.g., to reverse the body's orientation. Practical applications of microscopic robots may require rapid reorientations. Previous experiments have demonstrated that the robots can be steered by exerting a torque with electric and magnetic fields [11,12]. However, these robots are steered and controlled externally; a fully autonomous microrobot must be capable of responding adequately to changes in its local environment, with minimal external force or torque.

Here we turn to nature for inspiration, focusing on the rotational maneuvers of copepods, a common group of zooplankton thriving in the world's oceans and lakes. Maneuverability is crucial to the survival of adult copepods and their offspring (nauplii). A diversity of behaviors has been described in nauplii, which range from periods of immobility, swimming associated with foraging, and escape swims. Tracks of swimming trajectories in three dimensions have shown that, over time intervals in the range of minutes, nauplii typically move in helical patterns, using a stop-and-go pattern [13–16]. These authors also reported species-specific patterns, suggesting significant flexibility in behavior, despite the similarity in design. Copepods are under extreme predatory pressure from many aquatic organisms [17–19], and consequently, they have evolved remarkable escape responses to predatory attacks [15,20–24]. These responses often require a rapid reorientation to avoid swimming into the mouth of the predator [25]. Nauplii operate at lower Reynolds numbers than adults because of their smaller size, and they have a challenging task of capturing prey. While in later developmental stages, copepodids generate feeding currents, relatively few nauplii are able to do so [14]. Instead, nauplii swim toward their prey, generating a bow wave. In order to succeed in capturing the prey, a nauplius encircles the prey to draw it to the mouth while maneuvering its appendages [26]. While it is known that three pairs of appendages are involved, the details of appendage movements have not been resolved. Crustacean nauplii have three pairs of appendages that beat at a range of frequencies, with maximum frequencies recorded in copepod nauplii (>100 Hz; [27]). The asynchronous beating of appendages has been recognized as a factor for translating the body [5,6,28,29], and asymmetry in the appendage movement has been identified as a factor for reorienting the body [26]. However, the causal relationship between the movements of the body and the appendages and the resulting orientation remains unclear. Thus, the basic physical mechanisms behind the maneuvers have not yet been identified.

This work characterized the rotation of copepod nauplii around three perpendicular axes, as defined with respect to their body. For the rotation around each axis, we observed a sequence of movements of the appendages. Additionally, the tail moved considerably during the rotation around one of the axes. We interpreted these observations by using basic physical arguments and identified plausible mechanisms driving the rotation around each axis. Our findings suggest that, as the nauplius grows and develops a more pronounced tail, it gains an additional and efficient way of reorienting by performing a backflip somersault. Without the ability to rotate directly around one axis, the earliest stages of nauplii would need a strategic combination of rotations around the other two axes, in order to maneuver in three-dimensional space.

2. Materials and Methods

2.1. High-Speed Videography of Nauplii Swimming

Two species of Paracalanid copepods, *Bestiolina similis* and *Parvocalanus crassirostris*, were isolated from Kaneohe Bay (Oahu, Hawaii) and cultured by using the methods described in a previous study [30]. Temperature and salinity were maintained between 23 and 25 °C and approximately 35 ppt, within

the typical conditions of Kaneohe Bay [31]. The two species are comparable in size, developmental progression, and behaviors. They move intermittently in three dimensions. The nauplii (70–150 μm in size) were isolated from the cultures and gently pipetted into videography containers containing seawater and low densities of residual *Tisochrysis lutea*. We used two different methods for observing the nauplii: one from the side and another from above. The view from above was magnified by using 10 \times and 40 \times objective lenses of an inverted microscope (Olympus IX73). A small Petri dish (54.5 mm diameter) containing the nauplii was shifted horizontally, until a nauplius appeared in the field of view of the microscope. The second apparatus consisted of a cuvette (10 \times 10 \times 45 mm) containing the nauplii viewed from the side and magnified by comparable amounts, using an objective and condenser lens. We observed similar behavior and results from the side as from above. All videos were recorded with a high-speed camera (Phantom Miro M110), at frame rates between 1000 and 2000 fps; a total of 95 maneuvers were recorded.

2.2. Video Analysis

The videos were analyzed by using ImageJ software. Rotational maneuvers were analyzed frame by frame, and the rotations were categorized into three general types: yaw, roll, and pitch. The orientation of the body was determined by observing the plane formed by the appendages, the location of the labrum, and the direction of the curved tail. The labrum, or mouthparts of the nauplii, are located ventrally, and the tail curves toward the labrum. The appendage plane gives a sense of how the ventral/dorsal sides are oriented, while the labrum and curvature of the tail help to identify the ventral side of the body. The orientation could also be determined by tracking the motion of the nauplius throughout its maneuver and observing any appendage crossover during the rotation. Selected videos were analyzed by using Tracker and Microsoft Excel software. Tracker was used to track the body's midpoint and the endpoint of each appendage. The change of appendage angles with respect to the nauplius's initial heading direction was computed in Excel.

3. Results

3.1. Overview

Nauplii of *B. similis* and *P. crassirostris* were observed to rotate around three different axes. Figure 1 shows the axes and general anatomy of the nauplius. Nauplii have three pairs of appendages: antennules (A1), antennae (A2), and mandibles (M). The axes were defined such that the roll axis is along the length of the body; the pitch axis extends across the body, toward the right-hand side of the body, as perceived from the body; and the yaw axis is perpendicular to the plane formed by the pitch and roll axes, pointing in the direction from the ventral to the dorsal side of the body. During swimming, the appendages oscillate approximately in the plane containing the roll and pitch axes, at a frequency on the order of $f \sim 100$ Hz, corresponding to a duration of $T \sim 10$ milliseconds every periodic cycle. The appendages generate fluid flow at Reynolds number $Re = L(L/T)/\nu \sim 0.3$, where $\nu \sim 1 \text{ mm}^2 \text{ s}^{-1}$ is the kinematic viscosity of water at room temperature, $L \sim 0.05$ mm is the length scale set by the average length of all appendages, and L/T is the velocity scale. The Reynolds number is less than 1, meaning that the rotational motion of the nauplii is governed primarily by viscosity and less by inertia.

Our results depend greatly on the developmental stage of copepod nauplii. There are six nauplius stages (N1–N6); the first stage (N1) is the smallest and has a nearly spherical shape. The body becomes larger and more elongated in shape as it develops into later stages. Of the six nauplius stages, the first two stages, N1 and N2, are typically non-feeding [32]. The nauplii begin feeding at the N3 stage, which is distinguished from N1/N2 by the development of a noticeable tail. The nauplius stages were identified by using the shape and the length of the body and categorized as non-feeding (N1/N2) and feeding (N3–N6). The feeding stages are referenced as $\geq N3$ throughout the rest of this paper. The relative occurrences of all three rotations are shown in Table 1. Some videos showed rotations around axes which were unclear; these were not included for simplification. Rotations about the yaw

and pitch axis by an angle less than 45° and roll rotations by an angle less than 90° were considered incomplete and were not counted in the dataset. The significance of the table is that the rotation about the pitch axis was not observed at the early stages (N1/N2), whereas the later stages ($\geq N3$) displayed rotations about all three axes. Despite the apparent limitations of N1/N2, the nauplii are capable of exploring in three-dimensional space, as we discuss further below. We first describe how the body moves during each rotation, starting with the yaw rotation.

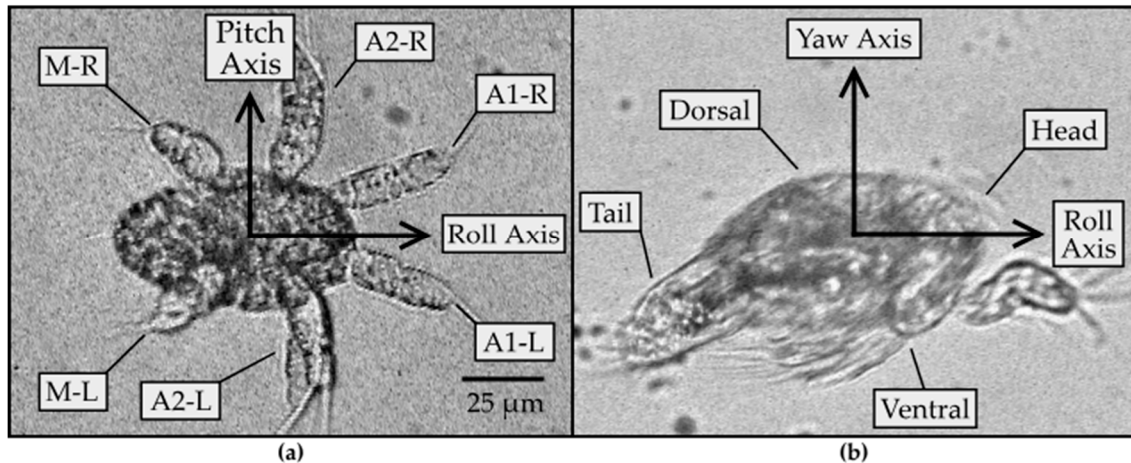


Figure 1. (a) Image of an N2 nauplius with the ventral side in view at $40\times$ magnification. The three pairs of appendages (antennules (A1), antennae (A2), and mandibles (M)) are each labeled L or R on the left or right side of the body, respectively. The pitch axis is defined to point in the direction from the left to the right side of the body; (b) image of $\geq N3$ nauplius at $40\times$ magnification. The roll axis points in the direction from the tail to the head end of the body. The yaw axis points from the ventral to the dorsal side of the body.

Table 1. Yaw, roll, and pitch occurrences by naupliar stage.

	Yaw	Roll	Pitch
N1/N2	10	21	0
$\geq N3$	15	19	30

3.2. Yaw Rotation

Figure 2 shows a time series and trajectory of a typical yaw rotation, which involves rotating around the yaw axis and turning toward one side of the body (see Supplementary Video 1). During this rotation, the midpoint of the body undergoes considerable back-and-forth translation in the plane perpendicular to the yaw axis. The net displacement of the body was measured to be $240 \pm 100 \mu\text{m}$ after rotating 180° around the yaw axis (mean and standard deviation, $n = 5$). The body alternates between moving forward (blue) and backward (red) along directions pointing approximately along the roll axis of the body. The directions of forward and subsequent backward motion are not precisely parallel; instead, they are offset systematically by a small angle, which leads to substantial turning after multiple cycles. The rotation efficiency was defined as the angular change in the orientation of the body every periodic cycle, and this was measured to be $33 \pm 6^\circ$ for yaw rotation (mean and standard deviation, $n = 5$).

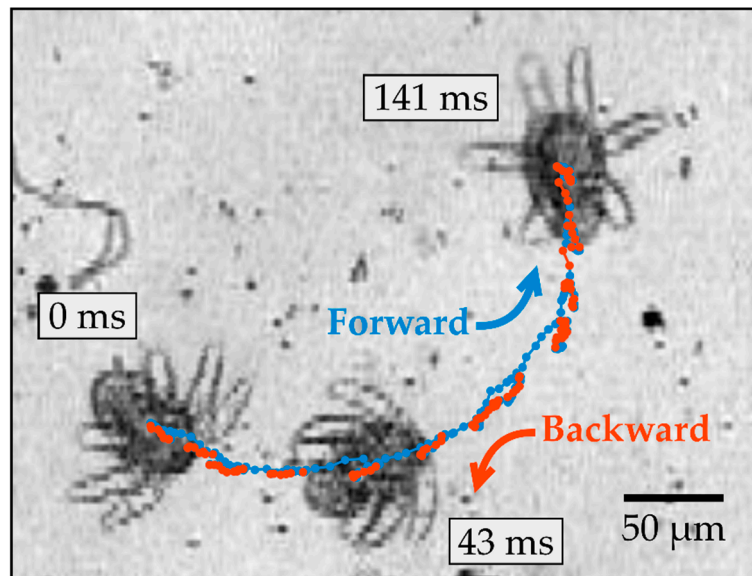


Figure 2. Time series of an N1/N2 nauplius undergoing yaw rotation observed at 10× magnification. The three snapshots of the nauplius were taken at different times, as indicated. The trajectory of the body’s midpoint is shown by dots, which are colored blue or red, depending on the direction of motion of the body.

To identify any left–right asymmetry in the movement of the appendages, we tracked the orientation of the body and all six appendages during the yaw rotation (Figure 3). The orientation of the body relative to its original orientation shows noticeable oscillations with time (Figure 3a). However, there is no apparent difference between the orientation of the appendages on the left and right sides of the body (Figure 3b).

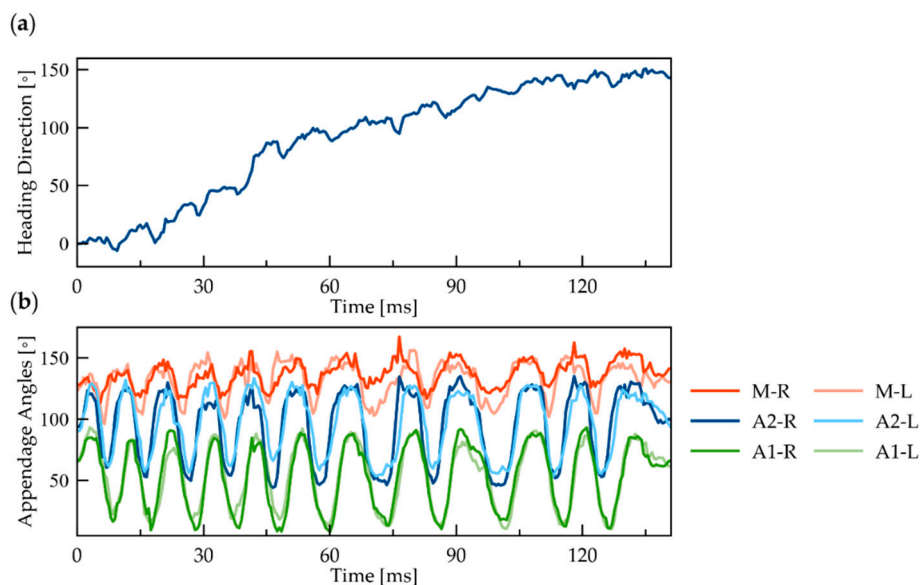


Figure 3. Yaw rotation of $\geq N3$ nauplius: (a) cumulative rotation over time of the body’s heading direction (roll axis) around the yaw axis; (b) temporal change in the orientation of six appendages, measured by the angle with respect to the body’s roll axis. Orange, blue, and green curves represent the M, A2, and A1 pairs, respectively. The light and dark colors correspond to the left and right sides.

To gain insight into possible mechanisms underlying the yaw rotation, we observed the nauplii at higher (40×) magnification, as shown in Figure 4 and Supplementary Video 2. Figure 4a reveals the

setae, flexible hair-like structures protruding from the distal tips of each appendage. These setae might fold or expand to different degrees on either side of the body, which would offer a possible mechanism for turning. However, we found no clear evidence of such asymmetry in the setae movement. Instead, we observed a noticeable asymmetry in the oscillation of the A2 appendages on the left and right sides of the body during the yaw rotation (Figure 4b). This was noticeable because the A2 appendage is biramous and splits into two branches. The two branches can appear to overlap if one lies above the other branch, as viewed in the direction parallel to the yaw axis. Alternatively, they appear as distinct branches if the appendage rotates by an angle close to 90 degrees around its long axis. This type of rotation is referred to as pronation or supination, depending on whether the branch on the ventral side swings toward or away from the body, respectively. The difference between pronation and supination was difficult to distinguish in our videos. Furthermore, the angle of rotation around the long axis of the appendage was difficult to quantify. Nevertheless, the two branches became more visible on the left but not on the right side of the body, indicating that the left appendage either pronated or supinated, while the right appendage did not. This implies that the rotated A2 appendage has a smaller profile area and thus drives less of the surrounding fluid on the left than the right during the important power stroke, which offers a possible mechanism for swerving the body to the left, as observed.

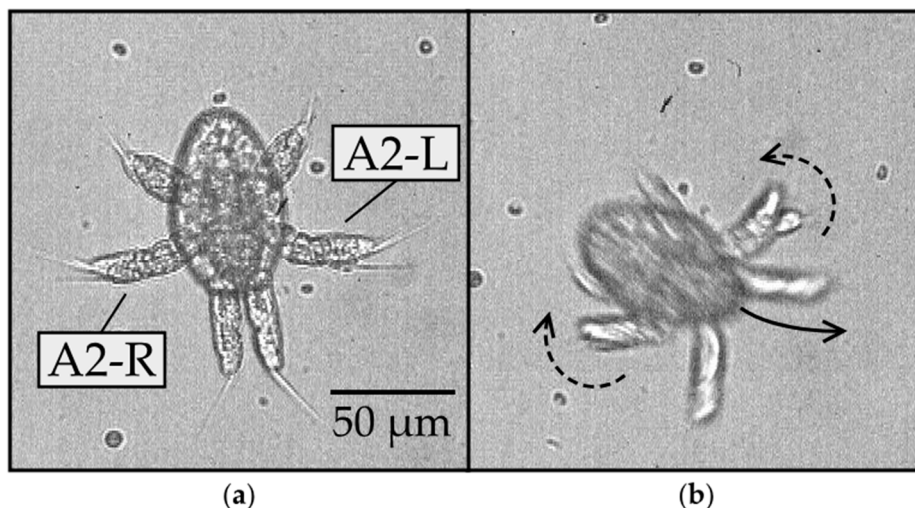


Figure 4. Yaw rotation of N1/N2 nauplius with the dorsal side in view at 40× magnification: (a) at the start of the rotation, the A2 appendages have branches appearing to overlap (0 ms); (b) as the body swerves to the left (counterclockwise), the two branches of the biramous A2 appendage become more visible in the left compared to the right A2 (21 ms).

3.3. Roll Rotation

Next, we describe the roll rotation, which involves the body rotating around the roll (main) axis while swimming along the axis. The body follows a helical path in a near-linear direction. The net displacement of the body after rotating around the roll axis by 180 degrees was measured to be $800 \pm 120 \mu\text{m}$ (mean and standard deviation; $n = 5$), which is considerably greater than the net displacement of the body following yaw rotation, as described earlier. During the roll rotation, the body alternates repeatedly between forward and backward displacements, which are comparable to those measured previously during linear swimming without rolling [6]. The large displacement of the body during the roll rotation makes it more challenging to observe the nauplii, because they only remain in focus for a brief period when they swim in and out of the field of view. Figure 5 shows a typical image sequence of a nauplius rotating around the roll axis by approximately 180° (see Supplementary Video 3). The right side of the body is initially in view, followed by the ventral side and then the left side. The rotation efficiency of the roll rotation was measured to be $27 \pm 6^\circ$, which is comparable to that of the yaw rotation described earlier.

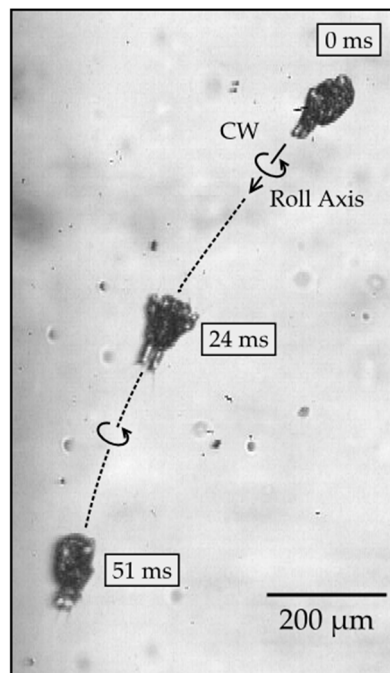


Figure 5. Time series of a roll rotation. Initially (0 ms), the right side of the body is in view, then the ventral side (24 ms), and then the left side of the body (51 ms).

The physical mechanism driving the roll rotation was difficult to visualize because of the challenges associated with observing the moving appendages in sufficient detail. A magnified view of the roll rotation showed that the appendages alternate between power and return strokes (see Supplementary Video 4), similar to appendage movements during the yaw rotation, as described earlier. There was no apparent explanation for how the roll rotation around the swimming direction was produced. Unlike the flexible cilia and flagella that are known to generate helical motion in swimming microorganisms [33,34], the appendages of copepod nauplii are rigid. One possible mechanism is that the tip of an appendage undergoes orbital motion as opposed to tracing the same curved path back and forth. This could repeatedly drive the surrounding fluid around the roll axis, though we observed no clear evidence of such orbital motion of appendages in our videos. Another possible mechanism is that an appendage pronates or supinates by an acute angle, which was more evident (see Supplementary Video 4). If an appendage remains pronated or supinated by an acute angle, say 45 degrees, during the power stroke, the appendage could drive the surrounding fluid around the roll axis and thereby resolve how the nauplii produce the roll rotation. The key is to produce left–right asymmetry, e.g., with pronation of the A2 appendage on the left or right side, but not both. This behavior was observed in all naupliar stages, including the early non-feeding stages.

3.4. Pitch Rotation

The pitch rotation produced relatively little translation of the body in three dimensions, enabling us to readily observe the rotation while the body remained in focus. The net displacement of the body after rotating around the pitch axis by 180 degrees was measured at $60 \pm 50 \mu\text{m}$ (mean and standard deviation; $n = 5$), with the smallest being $15 \mu\text{m}$ in the plane of the field of view. Figure 6 shows a typical image sequence of the rotation around the pitch axis by approximately 180° (see Supplementary Video 5). In the first image, the ventral side is in view, and the roll axis points toward the bottom-left corner of the image. In the second image, the tail end is in view, confirmed by the appendages on the ventral side appearing in the bottom-left corner of the image. Contrarily, if the head end were in view, the appendages would be located toward the top-right corner. In the third and final image, the dorsal side is in view. Thus, the body has flipped over by performing a backflip somersault. The rotational

efficiency of the pitch rotation was measured to be $60 \pm 30^\circ$ (mean and standard deviation; $n = 5$), which is much higher than those of the yaw and roll rotations presented earlier.

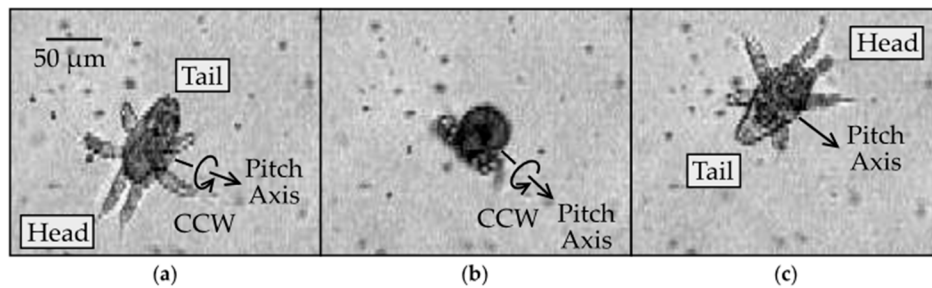


Figure 6. Image sequence of pitch rotation: (a) $\geq N3$ nauplius with ventral side in view (time $t = 0$); (b) tail end in view ($t = 10$ ms); (c) dorsal side in view ($t = 22$ ms).

Observations from one side of the nauplius along the pitch axis provided additional insights into the possible mechanism underlying the pitch rotation (Figure 7). The pitch rotation consists of the following sequence: contraction of the tail, contraction of the appendages, expansion of the tail, and expansion of the appendages, in this particular order.

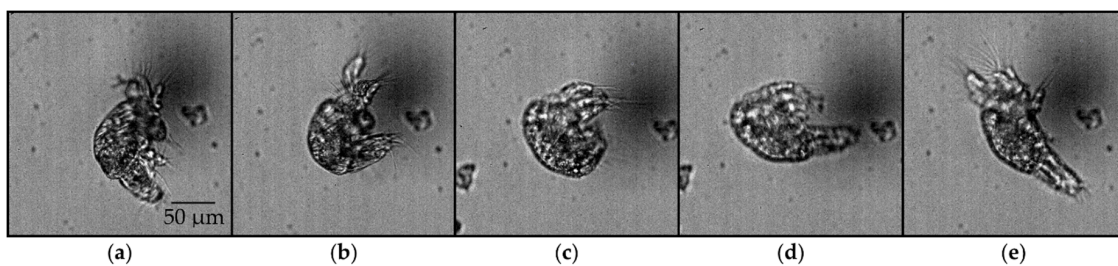


Figure 7. Image sequence of an $\geq N3$ nauplius undergoing pitch rotation, as viewed in the plane perpendicular to the pitch axis: (a) tail and appendages are expanded (0 ms); (b) appendages remained expanded, and tail was contracted (21 ms); (c) tail remained contracted, and appendages contracted (34 ms); (d) appendages remained contracted, and tail expanded (40 ms); (e) tail remained expanded, and appendages expanded (48 ms).

To understand why this particular appendage-and-tail-movement sequence results in the rotation of the body around the pitch axis, we consider a simplified theoretical model consisting of three slender rods connected in series by hinges, as sketched in Figure 8. Previous studies focused on the translation of the body, commonly known as Purcell’s swimmer [7,35]. Here we consider the rotation of the body. For simplicity, the six appendages are grouped into one end of the body, and the tail at the other. The rods do not incorporate the shape and movement of the tail and appendages in any quantitative detail, but they are sufficient for elucidating the basic effects of contracting and expanding the body parts in the particular sequence described before.

Suppose the two rods at the ends, hereafter referred to as the tail and arm of the body, are nearly parallel to the central rod initially (Figure 8a). First, the angle between the central rod and the tail is assumed to contract and close (Figure 8b). By conservation of angular momentum, the central rod rotates in the opposite direction to the tail, though the rotation angle is smaller in magnitude because the central rod experiences more drag than the relatively short tail. Second, the angle between the arm and the central rod is assumed to contract and close (Figure 8c). The arm and the central rod rotate in opposite directions by conservation of angular momentum again. However, the rotation angle of the arm is less than that of the tail in the previous step, because of the contracted tail. Third, the tail swings back open (Figure 8d). The rotation angle of the tail is equal to that of the arm in the previous step by symmetry. Fourth, the arm swings back open (Figure 8e). This has correspondence

with the time-reversal of closing the tail in the first step. After this entire sequence, the body rotates in the direction consistent with the experimental observations described earlier. Note that, without the ability to bend the tail, the simplified model would have only one hinge instead of two hinges. Such a body with only one degree of freedom would not be able to rotate at a low Reynolds number, which is consistent with the lack of observation of pitch rotations in N1/N2 nauplii.

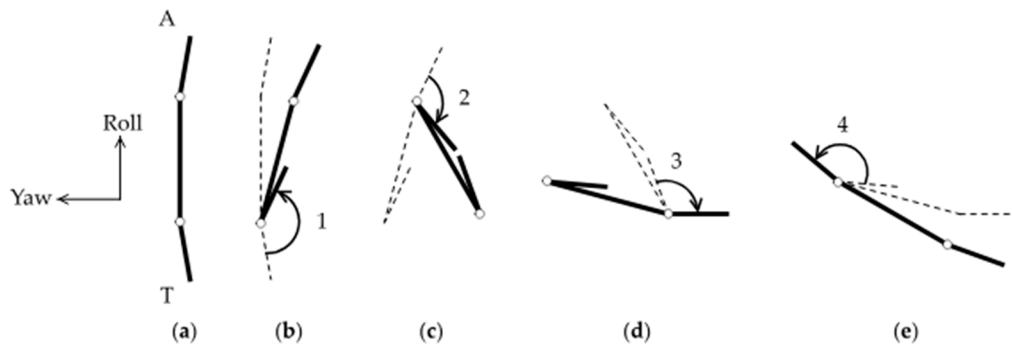


Figure 8. Simplified theoretical model for pitch rotation: (a) initial configuration of a body equipped with an arm (A) and a tail (T); (b) the tail closes and rotates by a large angle (1); the body rotates by a relatively small angle in the opposite direction. Dashed lines show the earlier configuration for comparison; (c) the arm closes and rotates by a moderate angle (2); (d) the tail opens and rotates by a moderate angle (3); (e) the tail opens and rotates by a large angle (4).

3.5. Direction of Rotation

The direction of rotation of the body was categorized into either clockwise (CW) or counterclockwise (CCW), according to the right-hand rule: CCW rotation around an axis is defined such that, if the right thumb points in the direction of the axis, as defined in Figure 1, then the right fingers curl in the same direction as the reorienting body. For example, a CCW yaw corresponds to a nauplius with the dorsal side in view, appearing to swerve to the left side of the body. A CCW roll corresponds to the body, with the head end in view, appearing to rotate around the roll (main) axis in the CCW direction. A CCW pitch corresponds to the body with the right side in view, appearing to perform a backflip.

Table 2 shows that the nauplii are capable of rotating in both directions around the yaw and roll axes. The number of observations in Table 2 is less than that in Table 1 because the ventral and dorsal sides were unclear in some videos, and thus the direction of rotation could not be determined in some yaw and roll rotations. Nonetheless, the result of pitch rotation is significant. The nauplii were observed to rotate around the pitch axis in the CCW direction only. The direction of rotation around the pitch axis was less ambiguous than the yaw and roll axes because the body remained in focus, with minimal translation during the maneuver. Additionally, the body orientations during the pitch maneuvers could be easily understood. For example, Figure 6b shows that the appendages located on the ventral side of the body are oriented more toward the initial heading direction (Figure 6a). This means that, regardless of whether the ventral or dorsal side is initially in view in Figure 6a, the body rotates around the pitch axis, with the ventral side facing outward. This corresponds to a backflip somersault with CCW rotation around the pitch axis.

Table 2. Clockwise and counterclockwise occurrences of yaw, roll, and pitch rotations.

	Yaw	Roll	Pitch
CW	10	12	0
CCW	8	14	30

4. Discussion

In summary, copepod nauplii exhibited rotations about three axes termed yaw, roll, and pitch. Naupliar stages N1/N2 were observed to perform yaw and roll rotations only, while \geq N3 nauplii were observed to rotate around all three axes. The pitch rotation was observed only in the CCW direction, meaning that \geq N3 nauplii were observed to flip backward, not forward. Most previous studies have examined the coordinated movement of the paired appendages, providing limited information on body rotation. Our observations are complementary to the studies and provide insight into how nauplii use their appendages to navigate in three-dimensional space.

The nauplius stage is widespread among the crustacea. While the organization of the naupliar body plan constrains movements, comparisons among nauplii from different crustacean groups have shown significant flexibility in locomotion [27]. Specifically, variations in morphology, the involvement of one vs. multiple pairs of appendages, and substantial differences in beat frequencies of the appendage(s) have been reported across taxa [27,36,37]. Copepod nauplii depend on locomotion to survive in an environment where predation risk is high, while food levels can be low. These nauplii are pelagic, capable of high-performance escape swims, and typically start feeding at the N3 stage [15,16,32,38]. The rapid escape swim is produced by the coordinated high-frequency (>100 Hz) beating of all three pairs of appendages (first antenna, second antenna, and mandible) [6,39]. Finding and capturing food is another challenge. For example, on a large scale, the nauplii of *Neocalanus* spp., in the subarctic North Pacific migrate vertically from depth (>200 m) to surface waters (0–50 m) to feed on the spring phytoplankton bloom [40]. At small spatial scales in the millimeter range, feeding behavior includes food-search strategies, as documented by 3D videography, which can be species-specific [14]. At the micrometer scale, the capture of an alga can involve a feeding current, as shown for *Eucalanus pileatus* [13] or more complex turning maneuvers to capture the alga, as shown for *Temora longicornis* and *Acartia tonsa*, using high-speed video [41].

While crustacean nauplii are small (<1 mm), the nauplii of the two target species in this study are among the smallest (length: 0.06 to 0.2 mm). These species operate at a low Reynolds number and require complex maneuvers to change the orientation of their body. Two of the rotations (yaw and roll) were observed in all naupliar stages (N1 to N6). These rotations allow the nauplii to change swim direction in three dimensions and contribute to the typical helical swim patterns described in other studies. Given that all naupliar stages are at risk for predation, the ability to redirect may add to their ability to evade predators. The third rotation, pitch, was only recorded in feeding stages (N3 to N6). The lack of a flexible tail in the N1/N2 may prevent these stages from completing the pitch rotation, which in turn may limit their ability to feed at low Reynolds number effectively. One might speculate that this may have led to the evolution of nauplii that depend on maternal resources to complete two molt cycles before they start to feed.

We conclude with a discussion of the space that is accessible to copepod nauplii and the implications for controlling microscopic robots that propel themselves autonomously. The ability to relocate from one position to another opens the possibility of reaching other positions in space, which depends importantly on the rotational maneuverability of the body. In general, the body does not remain perfectly axisymmetric around the direction of locomotion. Any minor left–right asymmetry in the shape or actuation mechanism prevents the body from following a straight line and instead turns the body to one side, as seen in the yaw rotation. Turning repeatedly to only one side would confine the body to loop around the same circle over time. The ability to yaw freely in either CW or CCW direction is important because it enables the body to escape from the circle and explore any point in the two-dimensional plane perpendicular to the yaw axis. Furthermore, to explore outside this plane, the body must rotate around another axis, e.g., the roll axis. The earliest stages of copepod nauplii display the ability to yaw and roll, and they can be executed in theory by the pronation or supination of a single biramous appendage that splits into two branches, as described here. Despite the apparent inability of the earliest stages of nauplii to rotate directly around the third (pitch) axis, they can explore three-dimensional space in principle. For example, the result corresponding to a

CCW pitch rotation by 90 degrees could be achieved by a time-consuming combination of yaw and roll rotations along a spiral path, e.g., a sequence of 90-degree CCW yaw, CW roll, and CW yaw rotations, in that order. The benefit of growing and developing a flexible tail in the older feeding stages of nauplii is that a similar result to such a sequence can be achieved more efficiently by rotating directly around the pitch axis. The strategies adopted by nauplii are excellent sources of inspiration for designing robots capable of navigating autonomously at microscopic scales. The robots may be configured to respond adequately to external cues, such as sudden changes in light or chemical gradients, with rapid acrobatic maneuvers, as observed in nature.

Supplementary Materials: The following are available online at <http://www.mdpi.com/2311-5521/5/2/78/s1>. Video S1: Yaw rotation. Video S2: Yaw rotation at higher magnification. Video S3: Roll rotation. Video S4: Roll rotation at higher magnification. Video S5: Pitch rotation. Video S6: Pitch rotation viewed parallel to the pitch axis.

Author Contributions: Conceptualization, K.T.M.N. and D.T.; data curation, K.T.M.N. and K.J.K.; formal analysis, K.T.M.N., K.J.K., L.N.B., P.H.L., and D.T.; writing—review and editing, K.T.M.N., L.N.B., P.H.L., and D.T.; funding acquisition, P.H.L. and D.T. All authors have read and agreed to the published version of the manuscript.

Funding: This research was funded by US National Science Foundation, grant numbers OCE-1235549, to P.H.L. and D. K. Hartline, and CBET-1603929 to D.T., and US Army Research Office, grant number W911NF-17-1-0442 to D.T.

Acknowledgments: The authors would like to thank Curtis Chan and Kyle Nugent for help providing the copepod nauplii, and Rudi Strickler for help setting up the side-view recordings.

Conflicts of Interest: The authors declare no conflict of interest.

References

- Bergou, A.J.; Ristroph, L.; Guckenheimer, J.; Cohen, I.; Wang, Z.J. Fruit flies modulate passive wing pitching to generate in-flight turns. *Phys. Rev. Lett.* **2010**, *104*, 148101. [[CrossRef](#)] [[PubMed](#)]
- Fish, F.E.; Nicasastro, A.J.; Weihs, D. Dynamics of the aerial maneuvers of spinner dolphins. *J. Exp. Biol.* **2006**, *209*, 590–598. [[CrossRef](#)] [[PubMed](#)]
- Lauga, E. Bacterial hydrodynamics. *Annu. Rev. Fluid Mech.* **2016**, *48*, 105–130. [[CrossRef](#)]
- Goldstein, R.E. Green algae as model organisms for biological fluid dynamics. *Annu. Rev. Fluid Mech.* **2015**, *47*, 343–375. [[CrossRef](#)] [[PubMed](#)]
- Gemmell, B.J.; Sheng, J.; Buskey, E.J. Compensatory escape mechanism at low Reynolds number. *Proc. Natl. Acad. Sci. USA* **2013**, *110*, 4661–4666. [[CrossRef](#)] [[PubMed](#)]
- Lenz, P.H.; Takagi, D.; Hartline, D.K. Choreographed swimming of copepod nauplii. *J. R. Soc. Interface* **2015**, *12*, 20150776. [[CrossRef](#)]
- Purcell, E.M. Life at low Reynolds number. *Am. J. Phys.* **1977**, *45*, 3–11. [[CrossRef](#)]
- Dreyfus, R.; Baudry, J.; Stone, H.A. Purcell's "rotator": Mechanical rotation at low Reynolds number. *Eur. Phys. J. B* **2005**, *47*, 161–164. [[CrossRef](#)]
- Rizvi, M.S.; Farutin, A.; Misbah, C. Three-bead steering microswimmers. *Phys. Rev. E* **2018**, *97*, 023102. [[CrossRef](#)]
- Jalali, M.A.; Alam, M.R.; Mousavi, S. Versatile low-Reynolds-number swimmer with three-dimensional maneuverability. *Phys. Rev. E* **2014**, *90*, 053006. [[CrossRef](#)]
- Tottori, S.; Zhang, L.; Qiu, F.; Krawczyk, K.K.; Franco-Obregón, A.; Nelson, B.J. Magnetic helical micromachines: Fabrication, controlled swimming, and cargo transport. *Adv. Mater.* **2012**, *24*, 811–816. [[CrossRef](#)] [[PubMed](#)]
- Hosney, A.; Klingner, A.; Misra, S.; Khalil, I.S.M. Propulsion and steering of helical magnetic microrobots using two synchronized rotating dipole fields in three-dimensional space. In Proceedings of the 2015 IEEE/RSJ International Conference on Intelligent Robots and Systems (IROS), Hamburg, Germany, 28 September–2 October 2015; pp. 1988–1993.
- Paffenhöfer, G.A.; Lewis, K.D. Feeding behavior of nauplii of the genus *Eucalanus* (Copepoda, Calanoida). *Mar. Ecol. Prog. Ser.* **1989**, *57*, 129–136. [[CrossRef](#)]
- Paffenhöfer, G.A.; Strickler, J.R.; Lewis, K.D.; Richman, S. Motion behavior of nauplii and early copepodid stages of marine planktonic copepods. *J. Plankton Res.* **1996**, *18*, 1699–1715. [[CrossRef](#)]

15. Titelman, J. Swimming and escape behavior of copepod nauplii: Implications for predator-prey interactions among copepods. *Mar. Ecol. Prog. Ser.* **2001**, *213*, 203–213. [[CrossRef](#)]
16. Bradley, C.J.; Strickler, J.R.; Buskey, E.J.; Lenz, P.H. Swimming and escape behavior in two species of calanoid copepods from nauplius to adult. *J. Plankton Res.* **2013**, *35*, 49–65. [[CrossRef](#)]
17. Eiane, K.; Aksnes, D.L.; Ohman, M.D.; Wood, S.; Martinussen, M.B. Stage-specific mortality of *Calanus* spp. under different predation regimes. *Limnol. Oceanogr.* **2002**, *47*, 636–645. [[CrossRef](#)]
18. Turner, J.T. The importance of small planktonic copepods and their roles in pelagic marine food webs. *Zool. Stud.* **2004**, *43*, 255–266.
19. Sampey, A.; McKinnon, A.D.; Meekan, M.G.; McCormick, M.I. Glimpse into guts: Overview of the feeding of larvae of tropical shorefishes. *Mar. Ecol. Prog. Ser.* **2007**, *339*, 243–257. [[CrossRef](#)]
20. Svetlichnyy, L. Speed, force and energy expenditure in the movement of copepods. *Oceanology* **1987**, *27*, 497–502.
21. Alcaraz, M.; Strickler, J.R. Locomotion in copepods: Pattern of movements and energetics of *Cyclops*. *Hydrobiologia* **1988**, *167*, 409–414. [[CrossRef](#)]
22. Lenz, P.H.; Hartline, D.K. Reaction times and force production during escape behavior of a calanoid copepod, *Undinula vulgaris*. *Mar. Biol.* **1999**, *133*, 249–258. [[CrossRef](#)]
23. Buskey, E.J.; Lenz, P.H.; Hartline, D.K. Escape behavior of planktonic copepods in response to hydrodynamic disturbances: High speed video analysis. *Mar. Ecol. Prog. Ser.* **2002**, *235*, 135–146. [[CrossRef](#)]
24. Buskey, E.J.; Strickler, J.R.; Bradley, C.J.; Hartline, D.K.; Lenz, P.H. Escapes in copepods: Comparison between myelinate and amyelinate species. *J. Exp. Biol.* **2017**, *220*, 754–758. [[CrossRef](#)] [[PubMed](#)]
25. Robinson, H.E.; Strickler, J.R.; Henderson, M.J.; Hartline, D.K.; Lenz, P.H. Predation strategies of larval clownfish capturing evasive copepod prey. *Mar. Ecol. Prog. Ser.* **2019**, *614*, 125–146. [[CrossRef](#)]
26. Bruno, E.; Andersen Borg, C.M.; Kiørboe, T. Prey detection and prey capture in copepod nauplii. *PLoS ONE* **2012**, *7*, e47906. [[CrossRef](#)] [[PubMed](#)]
27. Williams, T.A. The nauplius larva of crustaceans: Functional diversity and the phylotypic stage. *Integr. Comp. Biol.* **1994**, *34*, 562–569. [[CrossRef](#)]
28. Takagi, D. Swimming with stiff legs at low Reynolds number. *Phys. Rev. E* **2015**, *92*, 023020. [[CrossRef](#)] [[PubMed](#)]
29. Hayashi, R.; Takagi, D. Metachronal swimming with rigid arms near boundaries. *Fluids* **2020**, *5*, 24. [[CrossRef](#)]
30. VanderLugt, K.; Lenz, P. Management of nauplius production in the paracalanid, *Bestiolina similis* (Crustacea: Copepoda): Effects of stocking densities and culture dilution. *Aquaculture* **2008**, *276*, 69–77. [[CrossRef](#)]
31. Bathen, K.H. *A Descriptive Study of the Physical Oceanography of Kaneohe Bay, Oahu, Hawaii*; Hawai'i Institute of Marine Biology (Formerly Hawai'i Marine Laboratory): Kaneohe, HI, USA, 1968.
32. Mauchline, J. *The Biology of Calanoid Copepods*; Academic Press: San Diego, CA, USA, 1998.
33. Jennings, H.S. On the significance of the spiral swimming organisms. *Am. Nat.* **1901**, *35*, 369–378. [[CrossRef](#)]
34. Crenshaw, H.C. A new look at locomotion in microorganisms: Rotating and translating. *Integr. Comp. Biol.* **1996**, *36*, 608–618. [[CrossRef](#)]
35. Becker, L.E.; Koehler, S.A.; Stone, H.A. On self-propulsion of micro-machines at low Reynolds number: Purcell's three-link swimmer. *J. Fluid Mech.* **2003**, *490*, 15–35. [[CrossRef](#)]
36. Williams, T.A. A model of rowing propulsion and the ontogeny of locomotion in *Artemia* larvae. *Biol. Bull.* **1994**, *187*, 164–173. [[CrossRef](#)] [[PubMed](#)]
37. Dahms, H.U.; Fornshell, J.A.; Fornshell, B.J. Key for the identification of crustacean nauplii. *Org. Divers. Evol.* **2006**, *6*, 47–56. [[CrossRef](#)]
38. Titelman, J.; Kiørboe, T. Predator avoidance by nauplii. *Mar. Ecol. Prog. Ser.* **2003**, *247*, 134–149.
39. Wadhwa, N.; Andersen, A.; Kiørboe, T. Hydrodynamics and energetics of jumping copepod nauplii and copepodids. *J. Exp. Biol.* **2014**, *217*, 3085–3094.

40. Mackas, D.L.; Tsuda, A. Mesozooplankton in the eastern and western subarctic Pacific: Community structure, seasonal life histories, and interannual variability. *Prog. Oceanogr.* **1999**, *43*, 335–363. [[CrossRef](#)]
41. Borg, M.A.; Bruno, E.; Kiørboe, T. The kinematics of swimming and relocation jumps in copepod nauplii. *PLoS ONE* **2012**, *7*, e47486. [[CrossRef](#)]



© 2020 by the authors. Licensee MDPI, Basel, Switzerland. This article is an open access article distributed under the terms and conditions of the Creative Commons Attribution (CC BY) license (<http://creativecommons.org/licenses/by/4.0/>).